Polymer Testing 125 (2023) 108133

Contents lists available at ScienceDirect

Polymer Testing

journal homepage: www.elsevier.com/locate/polytest

Modeling and measuring the bonding strength of overmolded polymer parts

Anna Szuchács [a], Tatyana Ageyeva [a,b], József Gábor Kovács [a,b,*]

[a] Department of Polymer Engineering, Faculty of Mechanical Engineering, Budapest University of Technology and Economics, Műegyetem rkp. 3., H-1111, Budapest, Hungary
[b] MTA-BME Lendület Lightweight Polymer Composites Research Group, Hungary

ARTICLE INFO

Keywords:
Bonding strength
Overmolding
Polymer bonding

ABSTRACT

Overmolding a polymer onto a polymer substrate is a versatile plastic processing technique already widely used in industry and has a high potential to customize mass-produced polymer parts. Even though the industry is ready for this technology, there are still no engineering calculation methods to predict the strength of overmolded parts. None of the available engineering software packages contains the modeling of bonding strength between a polymer substrate and an overmolded element of the same material. This is because the complexity and interdisciplinary nature of bonding and the lack of a unified adhesion theory. In this study, we developed a unique modeling method that can accurately predict the bonding strength of the interface formed between a substrate and an overmolded element for acrylonitrile butadiene styrene (ABS). The method combines the analytical modeling of reptation, the numerical modeling of overmolding, the modeling of tensile tests, and the verification of the obtained modeling results with the tested ones. Our method has an average accuracy of over 90%.

1. Introduction

The growing demand from various industries for high-performance thermoplastic polymers and their composites drives the development of so-called "hybrid" technologies, which integrate two processes to produce a single part [1]. Such a combination gives engineers greater design freedom [2], and it has economic motivation like the overmolding of bio-based materials [3]. It also enhances the structural performance and appearance of components [4,5], and even allows the customized mass production of thermoplastics [6,7]. One of the most developed hybrid processes is polymer–polymer injection overmolding (hereinafter referred to as overmolding), in which one material is molded onto a previously formed and solidified substrate.

Even though overmolding is a well-developed industrial process, ensuring proper bonding between the substrate and the overmolded component is a challenge [8]. Its importance increases exponentially with high-performance structures designed to withstand high loads. The strength of the interface achieved during overmolding depends on many factors. Such factors are the structure of the interface, the physical and chemical properties of the materials joined, and the processing parameters of overmolding, such as temperature, pressure, holding time, etc. (Fig. 1). The number of possible combinations of these factors is very great. Therefore, it is reasonable to use a modeling approach to predict bond strength and find optimal processing parameters for overmolding at an early design stage.

Injection molding is a well-known field of simulation [10–12], and several CAE packages are available for modeling this technology. However, no available simulation software contains the modeling of bond strength between a substrate and an overmolded component. This is because the formation of bonding is quite a complex process and requires an interdisciplinary approach. Also, there is no unified theory of adhesion. Our current understanding is that after wetting, adhesion between two materials occurs due to the following mechanisms: mechanical interlocking, molecular diffusion, electrostatic interaction, and chemical bonding [13]. These mechanisms act simultaneously, but the degree of their impact on the resulting bonding strength is different. Several studies have proved that the formation of bonding during overmolding between the same thermoplastic polymers is well described by the molecular interdiffusion or healing theory, more specifically, the reptation theory, which de Gennes proposed in the 1970s [14]. According to this theory, the macromolecules of a polymer are surrounded by a "tube", which is a steric border between them and other molecules.

* Corresponding author. Department of Polymer Engineering, Faculty of Mechanical Engineering, Budapest University of Technology and Economics, Műegyetem rkp. 3., H-1111, Budapest, Hungary.
E-mail address: kovacs@pt.bme.hu (J.G. Kovács).

https://doi.org/10.1016/j.polymertesting.2023.108133
Received 27 April 2023; Received in revised form 9 June 2023; Accepted 26 June 2023
Available online 28 June 2023

When the temperature of a polymer rises above a specific temperature (T_g or T_m), the molecule chain starts to leave the tube and entangle with other macromolecules, thus forming a bond. The time in which a whole molecule chain escapes from a tube is called reptation time. Several mathematical models based on the reptation theory have been proposed to describe the healing process and to estimate bonding strength between amorphous polymers. Among these models are the two models proposed by Bastien and Gillespie [15], an integral model proposed by Sonmez and Hahn [16], and the model of Yang and Pitchumani [17]. All these models are based on the calculation of the degree of healing (D_h), which is defined as the ratio of bonding strength and maximal bonding strength (the tensile strength of the material) and is a function of time and reptation time (Equation (1)).

$$D_h = \frac{\sigma_b}{\sigma_\infty} = f\left(t_i;\ t_{rep}(T)\right), \tag{1}$$

where σ_b is bonding strength, σ_∞ is the strength of a single-piece part, t_i is the time in a particular time step, t_{rep} is reptation time, and T is temperature.

Several approaches have been proposed to model the formation of the interface during overmolding. For example, Giusti and Lucchetta [18] investigated the effect of different process parameters on the bonding strength for an overmolded PP composite with the help of a Design of Experiments. They found that melt temperature and holding pressure increase bond strength, while mold temperature decreases it. In their other study [19], they used two analytical models to predict the bonding strength of an overmolded PP part: the non-isothermal healing model proposed by Bastien and Gillespie [15] and the self-diffusion model. Both models are based on the reptation theory. The authors proved that the non-isothermal healing model can predict bonding strength when reptation time is calculated during the first very short phase of the buildup of interface temperature. However, the prediction error for the proposed model ranged from 1% to 35%, which proves that the method is unstable. Akkerman et al. [20] developed and experimentally validated a predictive model for the interface strength between a thermoformed composite sheet and overmolded polymer elements. The authors coupled the proposed model with commercial software, with which they created composites and performed injection molding simulation. The novelty of their approach is that it takes into account the semi-crystalline nature of PP. The authors assumed that the degree of healing is equal to the degree of melting, which occurs at the maximum temperature of overmolding. However, the proposed model is simplified, and the simulation results only qualitatively agree with the test results. Lafranche et al. [21] examined interfacial adhesion in an overmolded three-layer structure polyamide 6/maleic anhydride grafted polypropylene/polypropylene (PA6/PP-g-MA/PP) through microscopic analysis, mechanical characterization, and an inter-diffusion model. They proved that the bonding between the PP-g-MA and PP layers is mainly governed by the interdiffusion mechanism, while between the layers of PP-g-MA and PA6 by chemical linking. The authors used the calculation of the self-diffusion coefficient with the 1D cooling simulation in the Comsol Multiphysics software. This way, they calculated the quadratic distance of diffusion through the whole thickness of the overmolded part. The calculated quadratic distance of diffusion was the same order of magnitude as the thicknesses measured by optical microscopy. Zhai et al. [22] used molecular dynamic simulation to investigate molecular diffusion across the interface and interfacial bonding energy during the overmolding of a semi-crystalline polymer. They proved that the joining energy at the interface increases as the thermal gradient decreases. Their explanation was that as the thermal gradient decreases, the crystallinity and spherulite size of PP increase, resulting in a higher strength of the interface. Interestingly, under the term "thermal gradient" the authors meant the difference between the temperature of the melt and the temperature of the mold. Moreover, to obtain different thermal gradients, the authors changed both the temperature of the mold and the temperature of the melt, which complicates the evaluation of the results. Lorenz et al. [23] developed a methodology for predicting bonding strength in overmolded PP composites using simulation data and created a numerical model of the bonding mechanism. They used the healing and intimate contact models to calculate the bonding strength of the interface. The authors used the time-dependent nodal values of temperature, pressure, viscosity, and contact time as input data to compute bonding strength. They averaged strength for the individual nodes to calculate the bond strength in a specific area.

The modeling methods discussed above are still not sufficiently accurate and robust. The difference between modeled and measured bonding strength is relatively high and usually exceeds 10%. The reason for this difference is assumptions and simplifications in modeling. For example, none of the above-mentioned studies considers the unevenness of temperature distribution at the interface, which can significantly influence the modeled degree of healing. In our latest study [1], we proposed a method to predict bonding strength for overmolded amorphous polymers, which combines finite element modeling (FEM) with analytical modeling based on the reptation theory. A distinct feature of the proposed method is that it considers the continuous changing of the temperature field of the bonding surface during overmolding. Although we proved that our method could adequately predict the bonding strength for ABS, PS, and PC parts, the difference between the predicted and measured bonding strength was almost 7%. The possible reason for this difference is that the method averages the degrees of healing for the whole interface and calculates the final bonding strength based on the average value of D_h. In real life, the degree of healing, which defines the strength of the interface, is not the same across and along the bonding surface, therefore "weaker" and "stronger" zones appear in the interface.

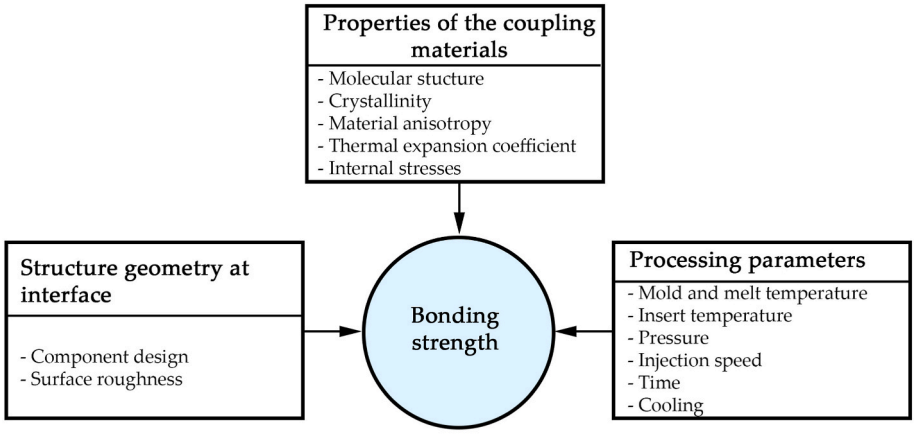

Fig. 1. Parameters that influence the bonding strength in overmolded structures (based on [9]).

During loading, the "weaker" zones start to fail first, thus decreasing the effective area of the interface. Due to accumulated damage, the measured failure load for the overmolded samples is usually lower than the modeled failure load. Two additional phenomena should be considered in the simulation of bond strength: the non-uniform distribution of the degree of healing across the interface and the related progressive damage of the interface under load. A new group of methods called progressive damage modeling (PDM) methods is used to trace damage propagation up to rupture in polymers [24] and composite materials [25]. In general, PDM includes stress analysis, failure analysis, and the calculation of the worsening of material properties. However, no single PDM method is suitable for all kinds of materials, although numerous PDM methods have been proposed in the last few decades [26]. One of the simplest PDM methods within the framework of conventional FEM is the element deletion method (EDM) [27]. Although the method is called an element deletion method, a certain element is not deleted, but instead, the stress in it is set to zero once it reaches ultimate stress [28]. EDM is more convergent than other PDM methods and requires less computing power [29]. EDM can be successfully used for the numerical modeling of crack propagation [28] and failure progression [29] in composites.

In this study, we combine the numerical modeling of the overmolding process, the analytical modeling of reptation, and EDM to develop a method to model bonding strength accurately in overmolded parts.

2. Material and methods

2.1. Experiments

2.1.1. Production of specimens

Three materials were used for the experiments. We used ABS Terluran GP35 (BASF, Germany, Ludwigshafen) in the injection molding and overmolding experiments, and in modeling the experiments. However, in order to show that the method works with other polymers, too, we performed experiments and modeling with polycarbonate (PC) Makrolon 2205 (Convestro AG, Switzerland) and polytyrene (PS) Edistir N 3910 (Versalis, Italy) as well. The results were good for both PC and PS. Production and prior drying were based on the values recommended by the manufacturer (Table 1).

For the characterization of the bonding strength between a base plate and an overmolded rib, we designed a so-called "T-shape specimen" (Fig. 2). It consists of an 80 mm × 80 mm × 2 mm injection molded base plate and a 70 mm × 63 mm × 2 mm rib, overmolded onto the base plate. An interface or a contact surface is formed between the base plate and the rib. The nominal dimensions of the contact area were 60 mm × 2 mm, excluding shrinkage.

We produced the specimens on an Arburg Allrounder 470 A 1000-290 (ARBURG Holding GmbH, Lossburg, Germany) injection molding machine. The "overmolded" specimens were manufactured in two steps, and each step needed a separate mold. We used a conventional two-cavity cold-runner injection mold for the first step (manufacturing the base plate). For the second step (overmolding), we used a specially developed mold equipped with a mechanically operated slider to put the base plate in its place (Fig. 3/b). Reference "single-piece" specimens

Table 1
Drying and molding recommendation for ABS Terluran GP35.

Material	ABS Terluran GP35	PC Makrolon 2205	PS Edistir N 3910
Drying temperature and time	80 °C for 4 h	120 °C for 2–3 h	not required
Recommended melt temperature range	220–280 °C	290–300 °C	200–250 °C
Recommended mold temperature range	30–60 °C	80–120 °C	1050 °C

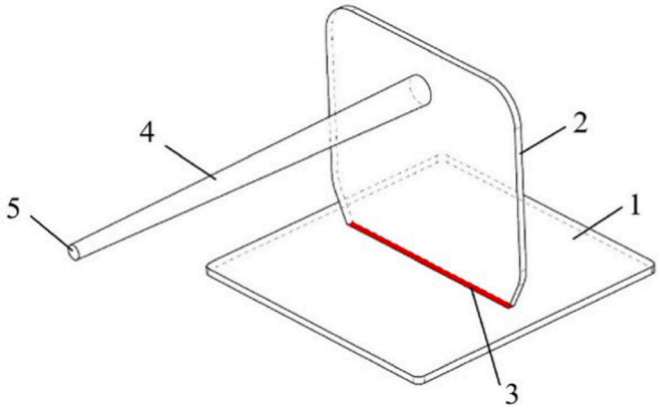

Fig. 2. T-shape test specimen: 1 – base plate (or substrate); 2 – overmolded rib; 3 – contact surface (or interface); 4 – sprue; 5 – injection point.

were produced with one-shot injection molding into a specially developed two-cavity cold-runner mold (Fig. 3/a). We produced 50 overmolded specimens, and 40 reference specimens.

The base plates and the overmolded ribs were manufactured with a melt temperature of 260 °C and a mold temperature of 40 °C. The injection rate was 32.5 cm^3/s. To control the switchover position, we installed a Cavity Eye RC15 pressure sensor (Cavity Eye Hungary Kft., Kecskemét, Hungary) into the wall of the mold. The pressure sensor was installed 10 mm before the contact interface. Switchover occurred when melt pressure reached 4 MPa. The resulting filling time, which was further used for simulations, was 0.6 s. The holding pressure was set to 75 MPa for 2.2 s, and the remaining cooling time was 20 s.

2.1.2. Mechanical testing

To determine the bonding strength of the interface, we performed tensile tests at room temperature with a Zwick Z020 universal tensile testing machine (Zwick Roell AG, Ulm, Germany) with a load cell limit of ±20 kN and a test speed of 5 mm/min. We used a special grip to fix the T-shape test specimen during the tensile test [1] (Fig. 4).

2.1.3. Rheological testing

To find the reptation time of ABS, we performed a frequency sweep test with a parallel plate rotational rheometer AR2000 (TA Instruments, New Castle, USA). The reptation time at a specific temperature is the reciprocal of the frequency when the elastic modulus (G') of the polymer is equal to its storage modulus (G'') (Fig. 5). The reptation time of ABS was measured at six different temperatures (150, 170, 190, 210, 230, and 250 °C) at frequencies from 0.1 to 600 rad/s. The shear strain was 0.5%, the diameter of the tested plates was 25 mm, and their thickness was 1.2 mm. The tested plates were cut from injection molded specimens.

We fitted the Williams-Landel-Ferry (WLF) equation (Eq. 2-3) on the measured values. With this fitted equation, we can calculate the reptation time at every temperature, not only at discrete values. Fitting yielded 6.22 for C_1 and 99.46 for C_2 at the reference temperature of 150 °C with a reference reptation time of 15.95 s.

$$\log a_T(T) = \frac{C_1(T - T_{ref})}{C_2 + (T - T_{ref})} \tag{2}$$

where $a_T(T)$:

$$a_T(T) = \frac{t_{rep}(T)}{t_{rep,ref}} \tag{3}$$

2.2. Simulations

Our ultimate goal is to create a model that accurately predicts the

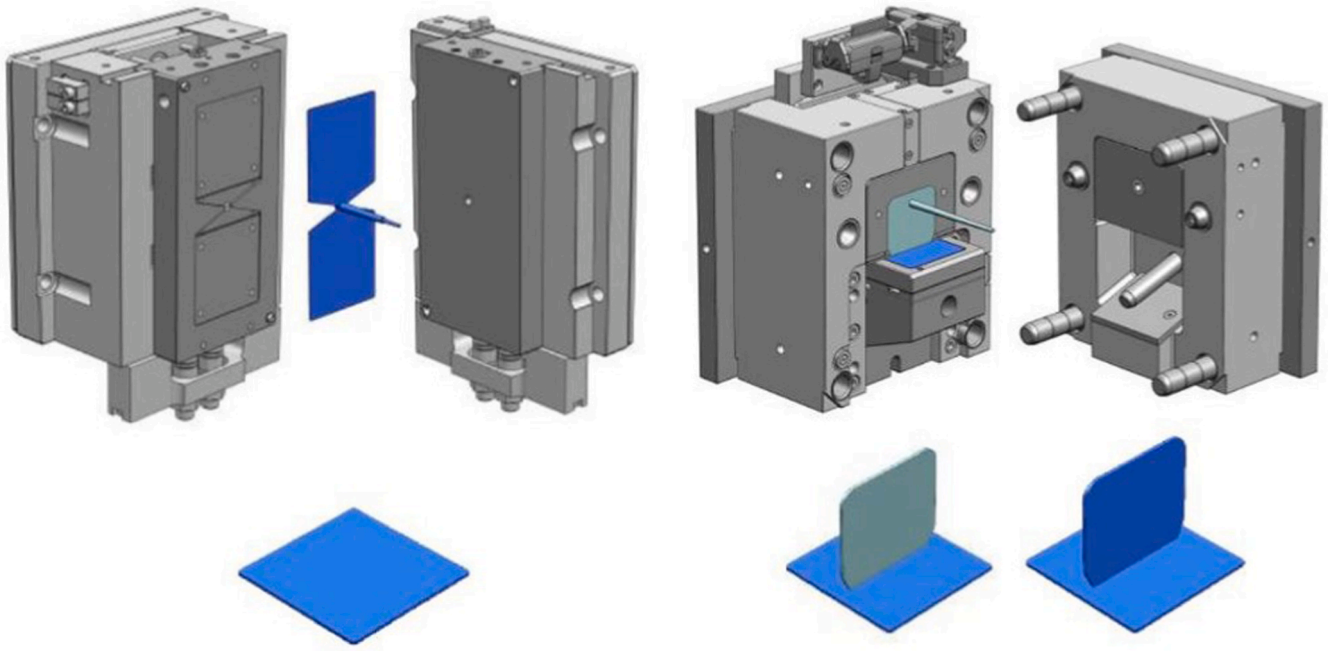

Fig. 3. (a) A two-cavity cold-runner mold for the production of base plates and (b) an injection mold for the production of T-shape test specimens (an overmolded and a single-piece specimen).

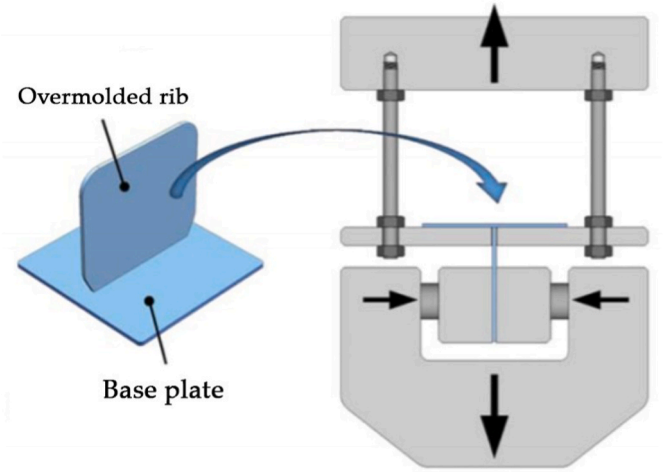

Fig. 4. Special grip for tensile tests.

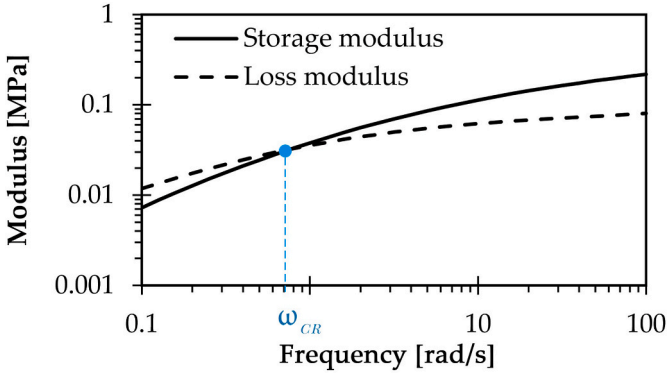

Fig. 5. The crossover frequency defined from the measured storage and loss modulus.

bonding strength in overmolded parts. For this purpose, we combined (1) the analytical modeling of reptation, (2) the numerical modeling of overmolding, (3) and the modeling of tensile tests based on the EDM method. A detailed description of the analytical modeling of reptation during overmolding is discussed in our recent study [1]. In the current research, we concentrate on the numerical modeling of overmolding and on the modeling of tensile tests, which can improve bonding strength simulation.

2.2.1. *Numerical modeling of injection overmolding*

We used the Moldex3D injection molding simulation software (Moldex3D Studio 2020) to model injection molding and overmolding. The values of the processing parameters were the same in the simulation as in our experiments. We used 3D tetrahedron elements to mesh the injection-molded T-shape part. The global element size of the T-shape part was set to 1 mm. To mesh the mold, we used a structured mesh. The areas of the mold in contact with the part were meshed with the same size of elements as the part. Further away from these regions, the mold was meshed with larger elements (Fig. 6). The injection overmolding simulation provided the temperature history of the individual node of the interface. The temperature history data was exported from Moldex3D to a.m3c file extension for further processing in Matlab.

2.2.2. *Simulation of the tensile test*

For the simulation of the tensile test, we used Matlab R2021b. As input data for Matlab, we used the temperature history data obtained during the numerical modeling of overmolding. However, the raw data of a simulation is in the.m3c format, which cannot be directly processed by Matlab. Therefore, data from Moldex had to be transformed. Fig. 7/a shows these transformations. First, the.m3c files are converted to a format that Matlab can interpret, the.txt format. The.txt file contains the temperature for each individual node at a certain timestep. The time steps in the.txt file are not quantitative values but just serial numbers in chronological order. To identify the temperature history of the nodes, we have to export the time values of each step into a.csv file. Another simulation run is required to identify the nodes that belong to the contact surface. In this simulation run, virtual constraints are placed on the nodes of the contact surface. The data of these nodes are saved in the.sbc

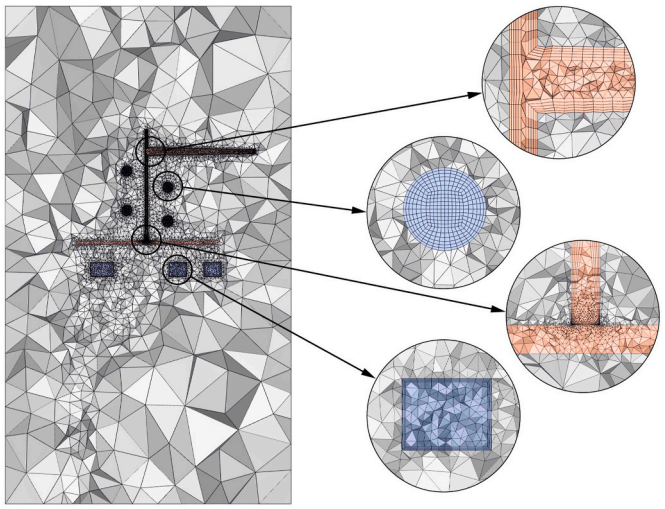

Fig. 6. Mesh of the cross-section of the mold and a T-shape part inside the mold used for the simulations.

format. A.sbc file contains the identifiers of the constrained nodes and allows matching temperature histories with the nodes. We then load the. sbc file into Matlab and isolate these nodes from the simulation. The coordinates of the nodes are also required. For this, the mesh of the model has to be in a processable form. In Moldex3D, there is an export option that saves the mesh in the file format.ans, which Matlab can read. This way, data obtained from Moldex3D with Matlab is processed with the use of four different data sources (Fig. 7/b).

2.3. Calculation

In FEM, every part is built up from elements and nodes (Fig. 8). Both elements and nodes can be used for the calculation of bonding strength between a substrate and an overmolded rib. However, the accuracy of calculation is affected by the geometric element chosen. In this study, we show how nodes and triangular elements can be used in the calculation of bonding strength and how total surface strength can be calculated from these elements.

From modeling, we obtain the strength distribution through all the individual elements or nodes of the contact surface. In most cases, the strength distribution obtained for individual elements and nodes must be converted into the bonding strength of the whole contact surface. The bonding strength of a contact surface is usually calculated by averaging the strength obtained for individual elements or nodes [19]. In our opinion, such an assumption does not describe an actual failure process and leads to an overestimation of bonding strength. Therefore, we have developed a new, more precise method to model a tensile test.

Using the measurements and simulation methods presented in the previous chapter, we calculated the bonding strength of a contact surface with four different methods (Fig. 9). We calculated the bonding strength of the interface by averaging the bonding strength of all the individual nodes (hereafter, we will call this calculation method "Method 1"). Then, by using the bonding strength of individual nodes, we modeled the tensile test and determined the overall bonding strength of the interface ("Method 3"). Method 2 is similar to Method 1 and Method 4 to Method 3; the only difference is that we used the bonding strength of the individual elements for the calculations in Methods 2 and 4.

2.3.1. Calculation of the degree of healing in nodes

The bonding strength of each node can be calculated with the healing equation developed by Yang and Pitchumani [17]. We use the reptation time to calculate the degree of healing, which has been proven to be applicable to the calculation [1]. To use reptation time, we need to know the temperature history in each node ($T_i(t)$) and the temperature-dependent reptation time of the material $t_{rep}(T)$:

$$D_{h,i} = \left[\int_0^t \frac{1}{t_{rep}(T_i(t))} dt \right]^{1/4} \tag{4}$$

The reptation time curve from time zero to the end of the process must be integrated for the calculation of healing. This reptation time curve (Fig. 10/a) can be calculated from the temperature history obtained from the injection molding simulations (Fig. 10/b) (Chapter 2.2.1) and from the measured temperature-dependent reptation time of the material with the transformed WLF equation (Fig. 10/c) (Chapter 2.1.3):

$$t_{rep}(T) = 10^{\frac{c_1(T-T_{ref})}{c_2+(T-T_{ref})}} \cdot t_{ref,rep} \tag{5}$$

Due to the nature of injection molding simulation, the results are obtained in discrete time steps. At each time step, each node has a discrete temperature value that corresponds to the reptation time of the material at that temperature. Integration can be performed after curve fitting or by the numerical integration of the points. The degree of healing results can be plotted, and so the weak points of the healing surface can be determined (Fig. 11). Fig. 11 shows that the degree of healing is lowest on the edges of the cross-section. These results correlate with those obtained in the study in Ref. [20].

2.3.2. Calculation of the degree of healing in the elements which belong to the contact surface

The surface area belonging to each node can vary even though the elements are of the same size. This is because the surface area which belongs to a node next to the wall is smaller than the surface area belonging to a node in the central part of the cross-section. Moreover, the surface area belonging to each node in the corners is even smaller (Fig. 12). The temperature is generally the lowest near the wall of the mold, so healing will also be weakest there (Fig. 11). Therefore, if the same surface area is assumed to belong to all nodes, the strength of the whole interface will be underestimated. This error can be avoided if the tensile test is calculated using the elements on the surface rather than the nodes. Using the elements on the surface requires some modifications compared to using the nodes.

The temperature history data are derived from the injection molding simulation results for each node. From the temperature history of the nodes connected to the elements, we calculated the temperature history of an individual element. At each time step, the temperature of the element is the average of the temperatures of the nodes connected to the element at that timestep (Equation (6)).

$$T_{e_k}(t_i) = \frac{\sum_{j=1}^{m} T_{n_{k,j}}(t_i)}{m} \tag{6}$$

where $T_{e_k}(t_i)$ is the temperature of the k^{th} element in timestep t_i, m is the number of elements connected to the k^{th} element, $T_{n_{k,j}}(t_i)$ is the temperature of the j^{th} node at timestep t_i, which is connected to the k^{th} element (Fig. 13).

We obtained the distribution of the degree of healing on the contact surface from the temperature history of the contact surface with the healing calculation equations used in the previous chapter (Chapter 2.1.1) (Fig. 14).

2.3.3. The calculation of bonding strength from the degree of healing

From the degree of healing, the bonding strength at a given point can be calculated with the use of the "infinite" bond strength. This value describes the strength that would be achieved if bonding time was infinitely long. If the material has an infinite time to bond, the material

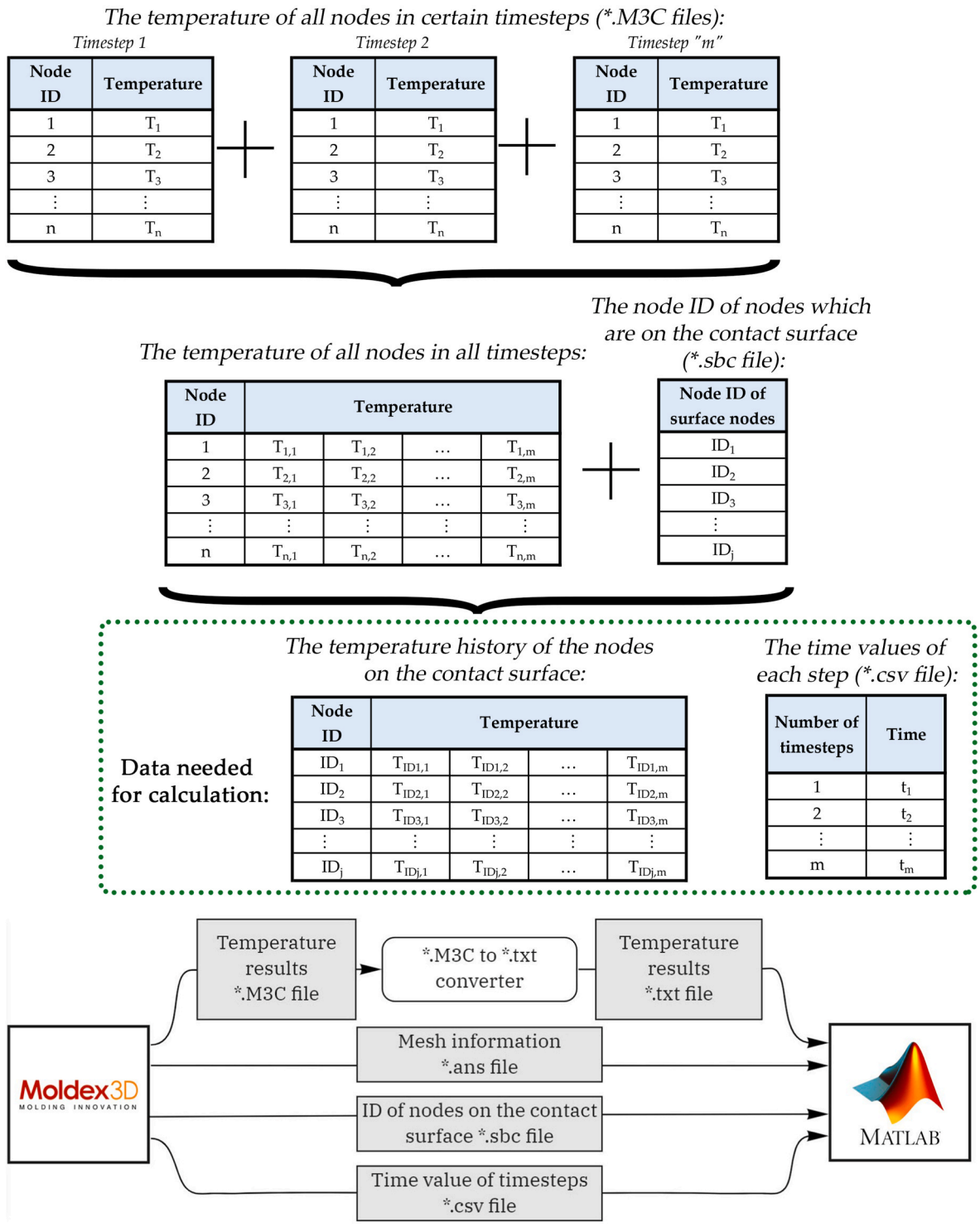

Fig. 7. Data transformation (schematically): (a) the creation of the data matrix needed for the calculations of the degree of healing; (b) transformation of files.

properties at the bond locations are the same as the properties of the bulk material. Therefore, we can use the tensile strength of the material as the "infinite" bonding strength (Equations (7) and (8)). To measure the tensile strength of the material, we produced a "single-piece" specimen (Chapter 2.1.1) and made tensile tests on it (Chapter 2.1.2).

$$\sigma_{n,j} = D_{h,n_j} \bullet \sigma_\infty \tag{7}$$

where $\sigma_{n,j}$ is the bonding strength of the j^{th} node, D_{h,n_j} is the degree of healing of the j^{th} node and σ_∞ is the tensile strength of the material.

$$\sigma_{e,k} = D_{h,e_k} \bullet \sigma_\infty \tag{8}$$

where $\sigma_{e,j}$ is the bonding strength of the j^{th} element, D_{h,e_j} is the degree of healing of the j^{th} element and σ_∞ is the tensile strength of the material.

2.3.4. Total bonding strength calculated by averaging

The calculation methods discussed in sections 3.1–3.3 give the bonding strength distribution of the contact surface. In studies focusing on the calculation of bonding strength, averaging is commonly used. For

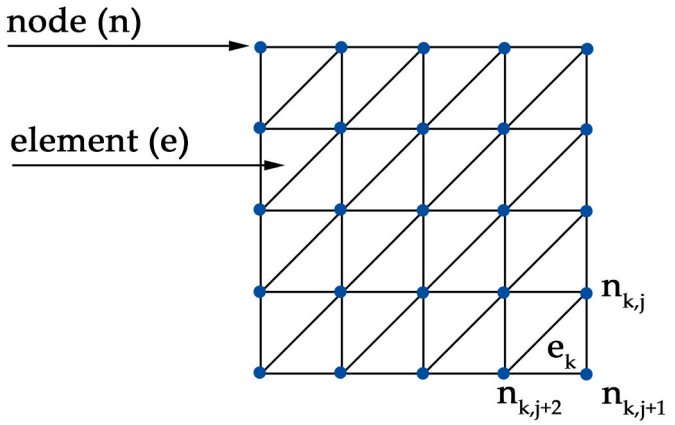

Fig. 8. The usual structure of the meshed surface and the notation of elements and nodes.

example, Giusti and Lucchetta [19] averaged the contact surface temperature, while Akkerman et al. [20] averaged the degree of healing. In both cases, the authors calculated the bonding strength of the interface using average values of either the temperature of the interface or the degree of healing. In reality, these assumptions lead to the overestimation of bonding strength, and therefore in these studies, the difference between modeled and experimental results exceeds 10%. In our current research, we first obtained the bonding strength distribution with the help of the individual nodes and elements. Then we calculated the bonding strength of the interface by averaging the bonding strengths of the nodes (Equation (7)) and the bonding strengths of the surface elements (Equation (9)).

$$\sigma_{t,n} = \frac{\sum_{j=1}^{i} \sigma_j}{i} \tag{9}$$

where $\sigma_{t,n}$ is the bonding strength of the total surface calculated from nodal bonding strengths, σ_j is the bonding strength of the j^{th} node and i is the number of nodes on the welded surface.

The bonding strengths obtained by averaging are not physically appropriate for calculating total bonding strength, and the average bonding strength calculated from nodes also introduces an additional error in the calculations since it does not take into account the fact that nodes are more densely distributed in some areas of the contact surface and less densely distributed in other areas. To correct this error, we used the bonding strength of the surface elements, where the strength values are weighted by the surface. To calculate the weighted average bonding strength, we need to know the area of the surface elements. This area can be calculated from the coordinates of the elements. The coordinates of the elements can be exported from any simulation software or meshing software. For triangular elements, the area of the triangle can be calculated from the coordinates as follows.

Coordinates of nodes connected to the element:

$$P_{n_{k,1}}(a_1, a_2, a_3), P_{n_{k,2}}(b_1, b_2, b_3), P_{n_{k,3}}(c_1, c_2, c_3)$$

The area of the triangle is:

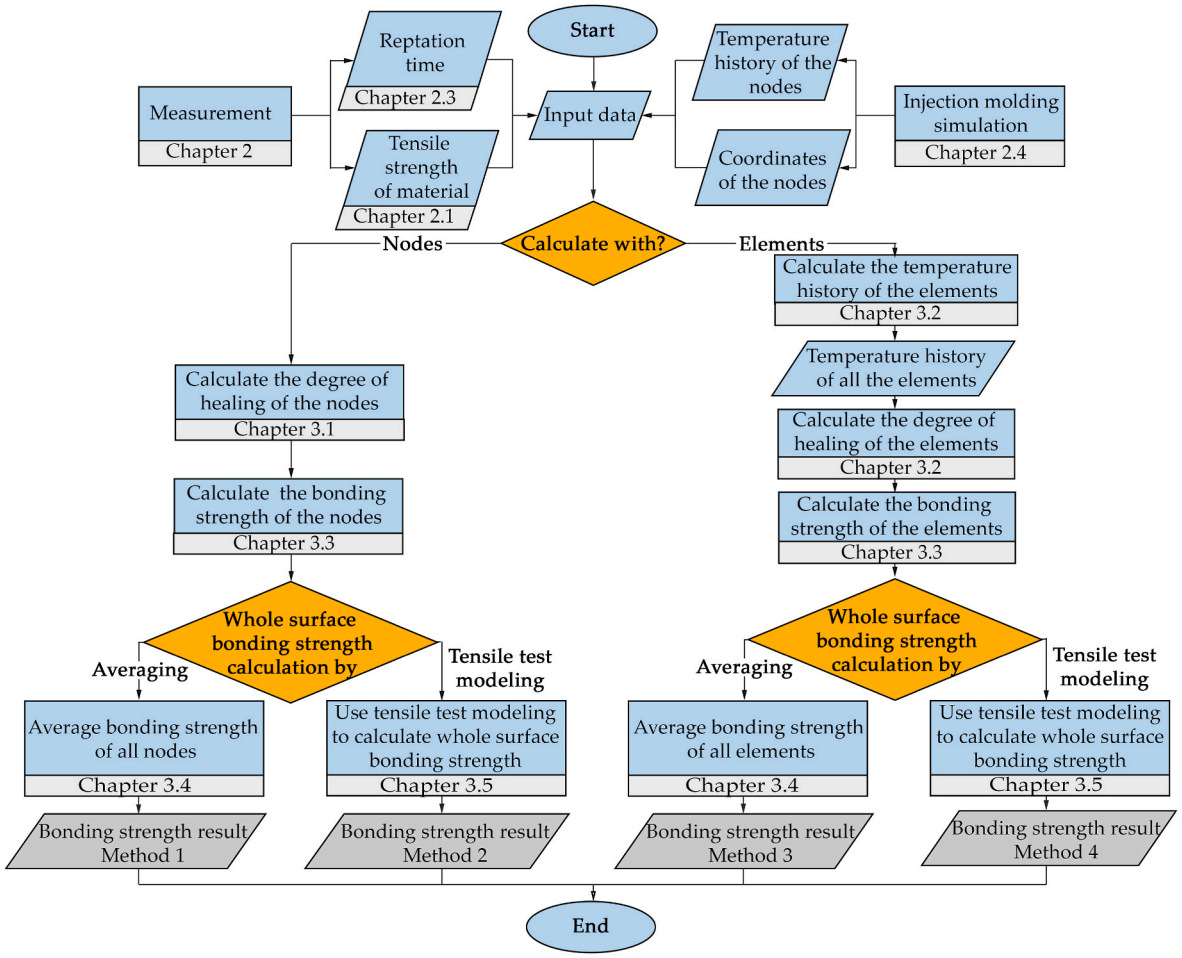

Fig. 9. The methods we developed for the calculation of the bonding strength of a contact surface between a base plate and an overmolded rib.

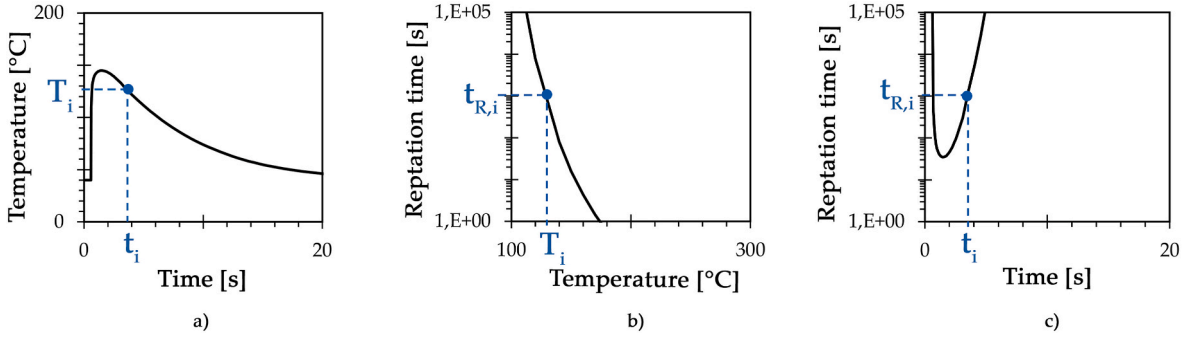

Fig. 10. The calculated (a) reptation time history of a node or surface element from (b) the temperature history and from (c) the temperature-dependent reptation time curve.

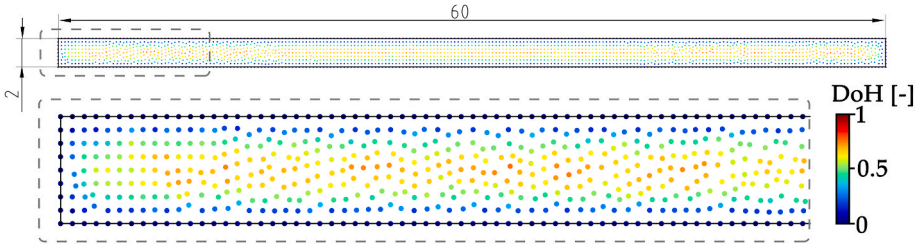

Fig. 11. Representation of the degrees of healing (DoH) on the welded surface calculated from nodal temperature values.

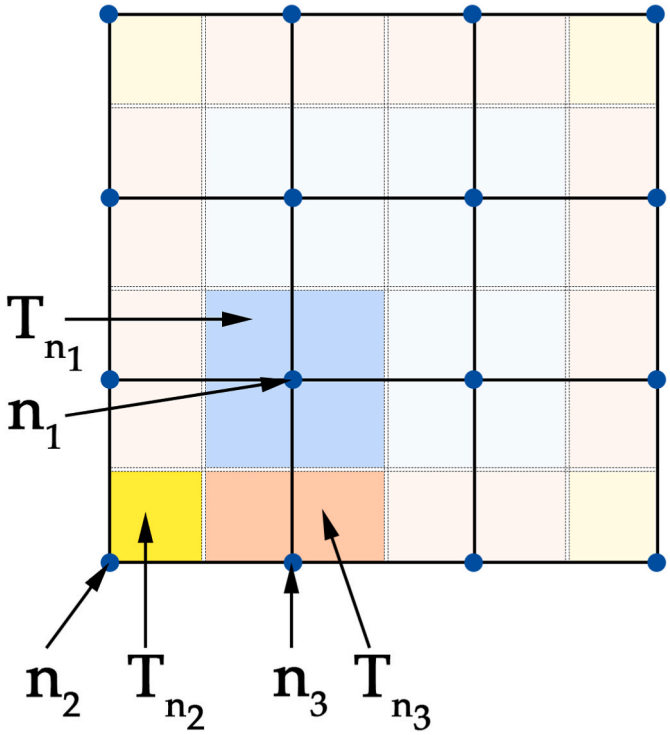

Fig. 12. The area which belongs to a node in the middle of the contact surface (blue), a node next to the wall (yellow), and a node in the corner (orange). (For interpretation of the references to colour in this figure legend, the reader is referred to the Web version of this article.)

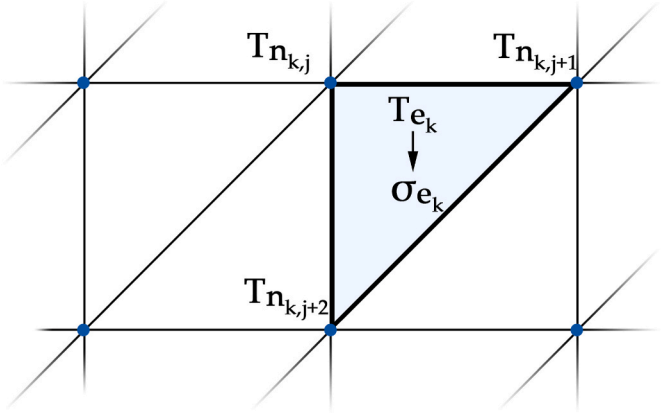

Fig. 13. The area of calculated bonding strength and the notation of the temperature of nodes and elements.

$$A_{e_k} = \frac{|\mathbf{u}|}{2}$$

Where **u** is

$$\mathbf{u} = \overrightarrow{\mathbf{P}_{\mathbf{n_{k,1}}}\mathbf{P}_{\mathbf{n_{k,2}}}} \times \overrightarrow{\mathbf{P}_{\mathbf{n_{k,1}}}\mathbf{P}_{\mathbf{n_{k,3}}}}$$

where $P_{n_{k,j}}$ is the coordinate vector of j^{th} a node connected to the element, and A_{e_k} is the area of the k^{th} element

$$\sigma_{t,e} = \frac{\sum_{k=1}^{z} \sigma_k * A_k}{A_{total}} \tag{10}$$

where $\sigma_{t,e}$ is the bonding strength of the total surface calculated from the bonding strength of the elements, σ_k is the bonding strength of the k^{th} element, z is the number of elements on the welded surface, A_k is the area of the k^{th} element and A_{total} is the area of the whole welded surface.

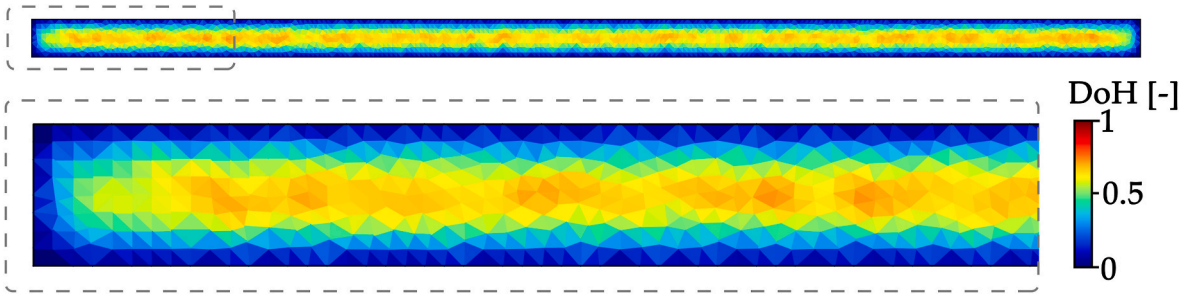

Fig. 14. The representation of the degrees of healing on the welded contact surface.

2.3.5. Modeling a tensile test

By modeling a tensile test, we can simulate the breaking process. Tensile testing can also be modeled with the bonding strength in nodes and the bonding strength in elements. The difference between the two calculations is that with nodes, the surface area that belongs to the node is not taken into consideration. It is assumed that the same surface area belongs to each node and that the bonding strength of these surface portions (Fig. 15) is equal to the bonding strength of the node. This assumption is correct if the size of the mesh elements on the contacting surface is nearly the same.

When modeling tensile testing, we aim to determine the maximum force that the specimen can withstand without breaking. As a simplification, we assumed that the same force was applied at each point on the surface, so the stress distribution is uniform. As the force was increased, the stress at the surface also increased, and at points where the stress exceeded the bonding strength of that point, that portion of the surface was broken. Because of the broken portions, the undamaged surface area decreased, so for the same force, the stress increased in the nonbroken parts of the surface. The force increased until the entire contact surface broke. In the last timestep, when the entire surface broke, the force that was pulling the surfaces apart became the maximum tensile force (F_{max}) used for calculations. The engineering strength (σ_{total}) can be calculated from this force (F_{max}) and from the initial area of the surface (A) (Equation (11)).

$$\sigma_{total} = \frac{F_{max}}{A} \tag{11}$$

To model tensile testing with surface elements, we need to know the bonding strength in the elements and the size of the elements. As with calculation for nodes, we assume that the force acting on the surface is uniform, so the stress on the surface is the same for all elements. When stress in an element exceeds the bonding strength of this element, the surface starts to break, and the total surface area decreases by the area of the failed element. Therefore, the area of the contact surface that carries the load progressively reduces, and the undamaged elements experience higher and higher stress. The tensile force increases until the entire contact surface breaks and the resulting maximum force is used to calculate the bonding strength of the entire surface.

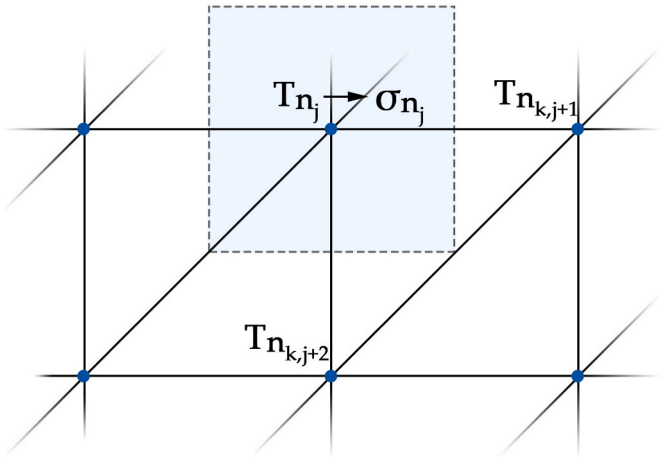

Fig. 15. The surface area of an individual node (blue area) when we use the bonding strength of the nodes to calculate the bonding strength of the whole surface. (For interpretation of the references to colour in this figure legend, the reader is referred to the Web version of this article.)

2.3.6. Modeling example

To illustrate the modeling of the tensile test, we use a contact surface of 3 by 3 square surface elements. Each surface element is 1 mm^2 in area, so the total surface is 9 mm^2. Let us assume that the calculated bonding strengths are as shown in Fig. 16.

Of the two methods, i.e., averaging and tensile test modeling, we first examined the total strength of the interface obtained by averaging. The surface consists of nine elements (Fig. 17/a). The strengths of these elements were averaged to give a total surface tensile strength of 1.78 MPa (Equation (12)).

$$\sigma_{total} = \frac{\sum_{i=1}^{n} \sigma_{N_i}}{n} = \frac{16}{9} = 1.78\ MPa \tag{12}$$

For tensile test modeling, the force on the surface increases, and the

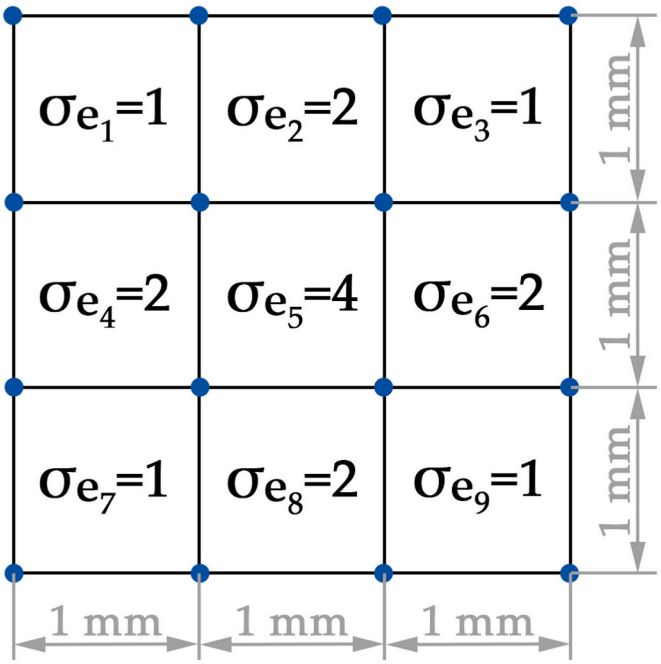

Fig. 16. Sample surface to illustrate tensile test modeling, where the number written in the surface element indicates the strength of the surface element in MPa.

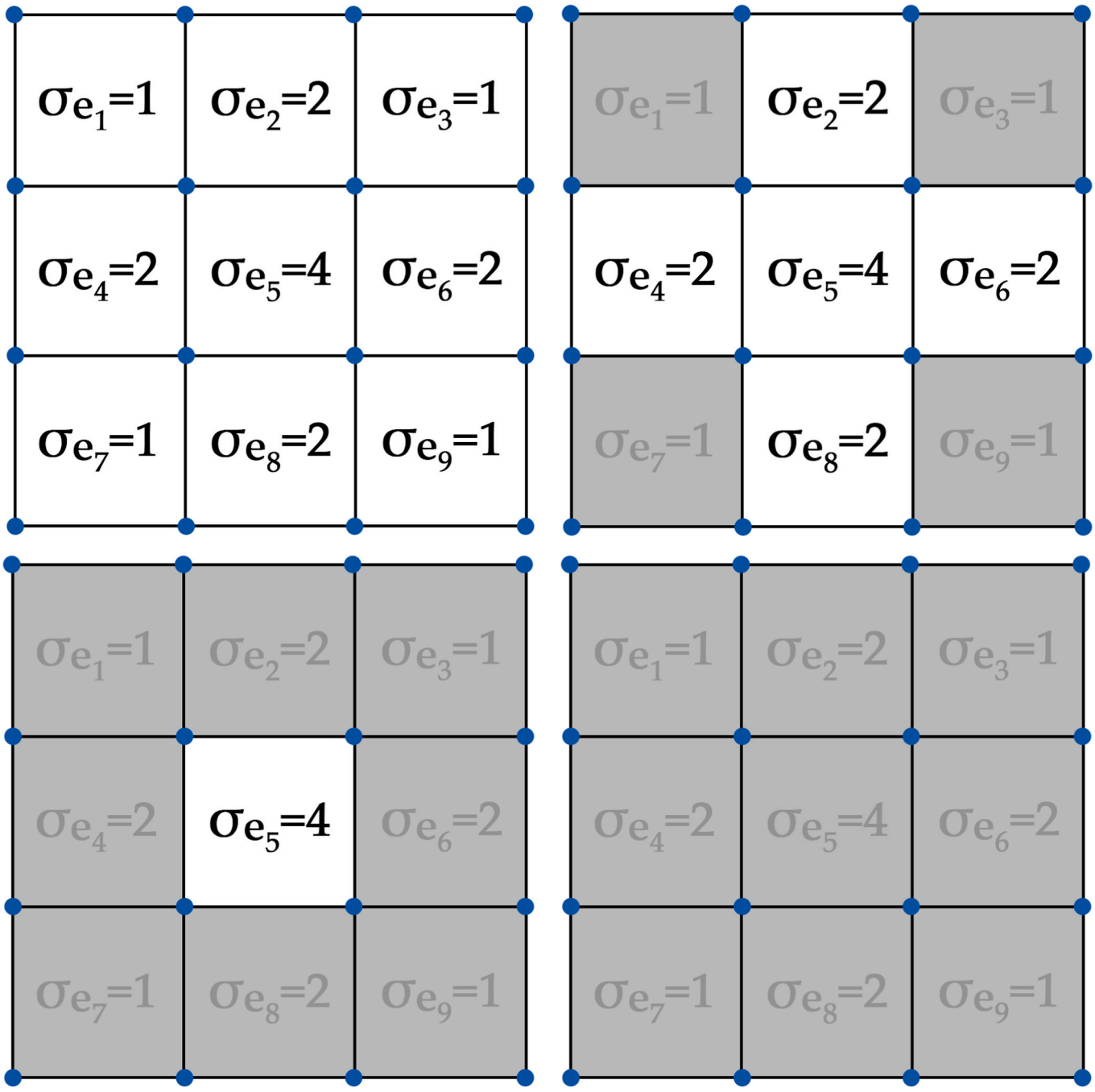

Fig. 17. The process of modeling the tensile test, (a) the initial, completely intact (white) surface, (b) surface portions that are broken by 9 N (grey), (c) surface portions that are broken by 10 N and (d) the entire surface that is broken by 10 N due to the reduced cross-section.

stress on the small surface units is calculated for each increase. If the calculated stress is greater than the bonding strength of a surface portion, that surface portion will break. The first surface element will break at 9 N (Fig. 17/b) since, at this moment, the tensile stress is 1 MPa on each surface element. An increase of tensile force to 10 N results in a stress of 2 MPa for the five remaining elements. As a result, 4 more elements break (Fig. 17/c). After this, the one remaining undamaged surface element will be subjected to a stress of 10 MPa and will break (Fig. 17/d). The surface can withstand a force of 10 N, divided by the initial cross-section, which gives a total surface strength of 1.11 MPa. We demonstrated that with this more realistic calculation method, the tensile strength which the interface of bonded parts can withstand is reduced by 60%.

3. Results

This section is dedicated to the validation of the modeling methods for the prediction of the bonding strength of the ovemolded specimens (Fig. 18).

The parameters of the mesh can significantly affect the calculation results. To investigate this effect, we created various meshes which differ in element size (Fig. 19).

After running the simulations in Moldex3D, we calculated the strength of the individual elements and nodes using temperature histories and the coordinates of the nodes in Matlab. The strength distributions over the nodes and elements of the contact surface were plotted, and these plots were used to show the weak points on the contact

Calculation method / Element used	Averaging	Tensile test modeling
Node	Method 1	Method 3
Surface element	Method 2	Method 4

Fig. 18. Methods of the modeling of bonding strength in an overmolded specimen.

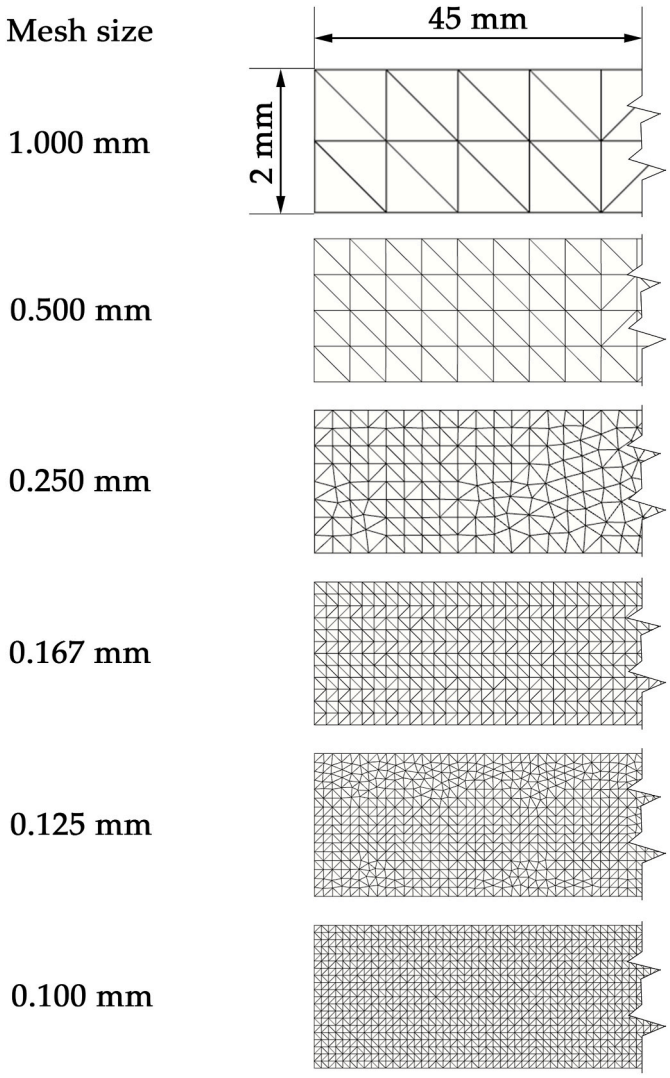

Fig. 19. Contact surface meshes with different parameters of the mesh (For a better visibility, only a tiny section of the meshed part is shown).

surface. It is more difficult to analyze the map of the degree of healing obtained from nodes (Fig. 20/a) as it does not give a continuous picture of the surface. Only the degree of healing at the node is displayed. On the other hand, the map of the degree of healing plotted with elements can be analyzed well (Fig. 20/b). As element size is reduced, the distribution of the calculated degree of healing becomes more and more detailed and accurate (Fig. 20).

3.1. Validation of method 1 and method 2

The strength of the whole contact surface was calculated by averaging the strength of the elements (Method 2) and the nodes (Method 1). The simplest method of obtaining the bonding strength of the whole surface is to average the bonding strength calculated for individual nodes (Fig. 14/Method 1). A similar method is to calculate the strengths of the surface elements and then average them weighted by area; this also gives the bonding strength of the total surface (Fig. 14/Method 2). We aim to show the significant error caused by averaging. The result greatly overestimates real bonding strength. This is because averaging gives the same weight to all points and surfaces, whereas in reality, it is the less bonded locations that determine strength. The nodal and surface element results are very similar because the surface has mesh elements of nearly the same size (Fig. 21). The reason for the difference between the results of the nodes and the surface elements is that the nodes next to the wall have the lowest strength. Since the nodes do not have a surface, we cannot take into account that these nodes have the smallest surface as well, so this reduces overall bonding strength (Chapter 2.3.2).

When the mesh elements on the surface are of different sizes, the total surface strength calculated with nodes and elements differs greatly. While bonding strength obtained with the elements (Method 2) is the same for equal and unequal element sizes, the strength calculated with nodes (Method 1) depends greatly on the meshing (the density of nodes) (Fig. 22).

This is because when element sizes are different, the nodes associated with smaller mesh elements are not given proportionally less weight. Therefore, if there are more elements in the warmer parts of the surface, the calculated total bonding strength will be higher than with an equally spaced mesh. In comparison, if there are more elements in the colder parts of the surface, the calculated strength will be lower (Fig. 23).

3.2. Validation of method 3 and method 4

In Methods 3 and 4, we modeled a tensile test to determine the bonding strength of the entire contact surface, using strength at the nodes for Method 3 and strength at the surface elements for Method 4. The bonding strengths delivered by Methods 3 and 4 are far more accurate than those provided by Methods 1 and 2 (Fig. 24). This is because these calculation methods (Method 3 and Method 4) track the breakage process while averaging (Method 1 and Method 2) cannot do so. The results obtained with nodes and elements are so close to each other because the element sizes at the contact surface were almost identical. Therefore, weighting by the size of the surface elements did not have a great influence. When we used the methods based on nodal calculations

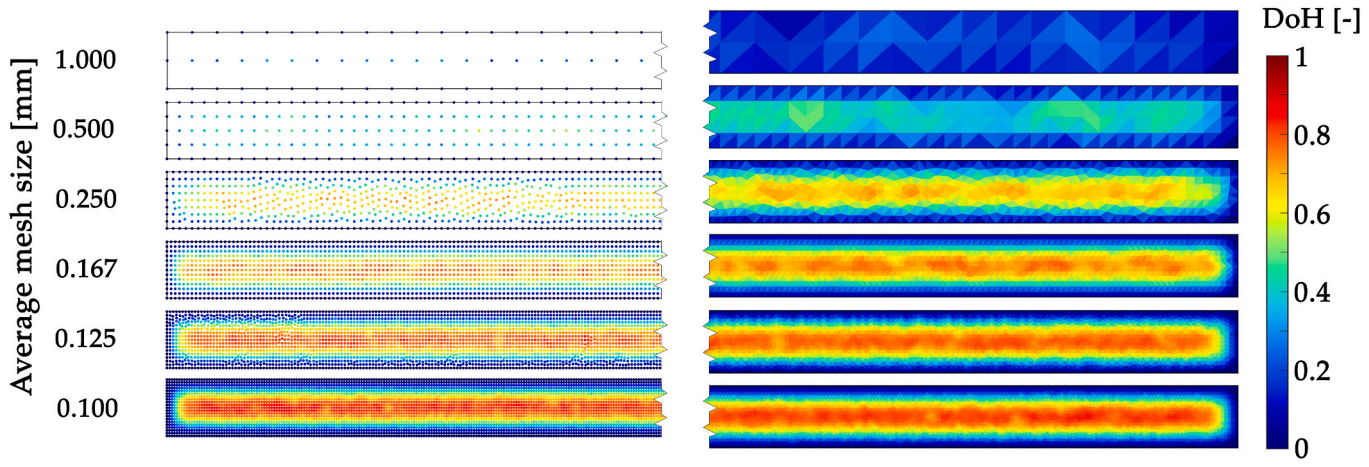

Fig. 20. The plot of the degree of healing calculated with (a) nodes and with (b) surface elements.

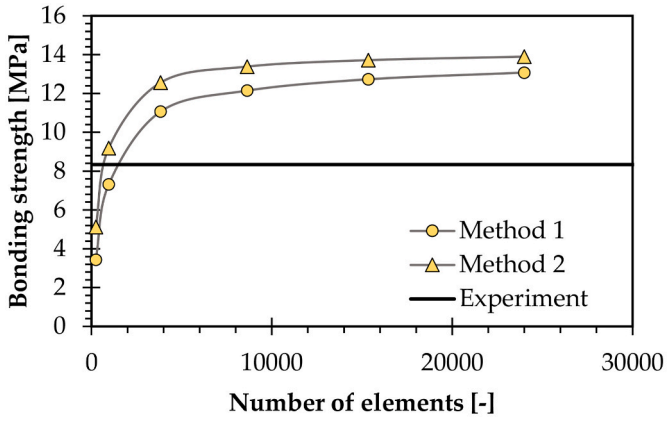

Fig. 21. Total bond strength calculated by averaging the strength in the nodes and elements with uniform element sizes.

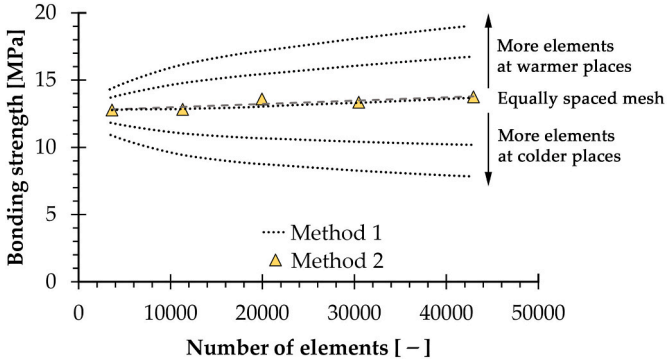

Fig. 22. Total bonding strength of a contact surface calculated by averaging the strength in nodes and elements with meshes of unequal element sizes.

(Method 1 and Method 3), we obtained lower values of bonding strength than in the case of element-based methods (Method 2 and Method 4). This is because the nodes adjacent to the wall of the mold have a smaller specific area than the nodes in the center of the contact surface (Fig. 12). This phenomenon is not considered in the calculation with Methods 1 and 3. Therefore, in this case, the lower temperature of the contact surface near the wall will reduce the calculated tensile strength of the entire contact surface (Fig. 24).

However, when the elements on the contact surface are of different

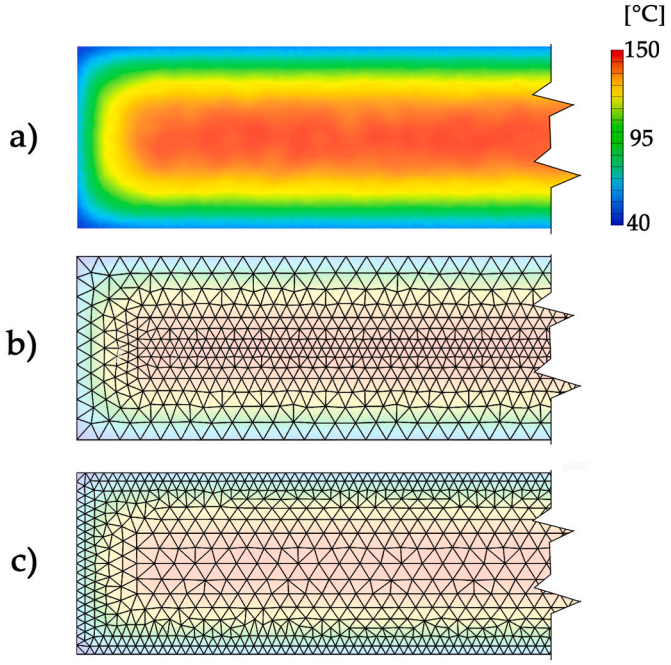

Fig. 23. (a) The temperature of the contact surface and the mesh (b) when there are more elements at the warmer places and (c) when there are more elements at the colder places.

sizes, the strength calculated with nodes is not accurate, even with tensile test modeling (Fig. 25). In this case, total tensile strength has to be calculated from the surface elements, as this approximates bonding strength most accurately.

We demonstrated that the presented method (Method 3) is sensitive to the size of the elements on the contact surface. When the size of the elements on the contact surface is not the same, the strength of the nodes should not be used for the calculations, as they are not weighted. With different mesh sizes, bonding strength should be calculated by tensile modeling with the strength of the interface elements (Fig. 26).

3.3. *Validation with other materials*

There can also be a considerable variation between the healing behavior of different amorphous materials, so we also tested our calculation method with polystyrene (Versalis Edistir N 3910) (Fig. 27/a) and polycarbonate (Convestro Makrolon 2205) (Fig. 27/b). To do

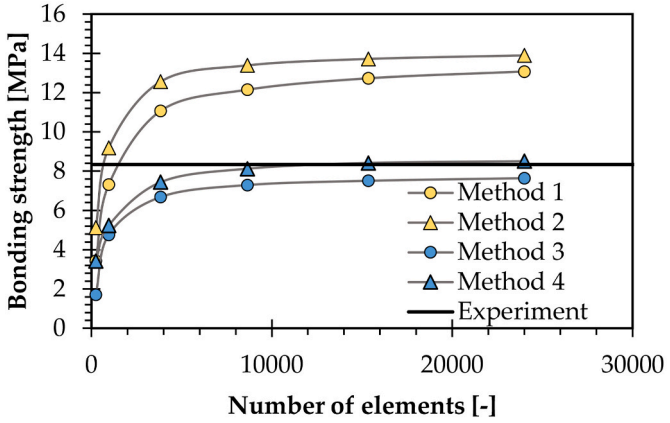

Fig. 24. Total bonding strength of the contact surface defined by Methods 1–4 for different numbers of mesh elements.

this, we manufactured test specimens that we can later use to validate our modeling results. We also measured the strength of a "single-piece" specimen for each material, which we used as the maximum strength in the calculation. Since melt temperature has the greatest influence on weld strength, we prepared specimens with different melt temperatures. We selected wide melt temperature ranges for all materials. In most cases, the calculated bonding strength is within the standard deviation of the measured result, and the calculation gave a good approximation in the examined range.

4. Conclusion

We developed a universal modeling method that can accurately predict the bonding strength of the interface which forms during overmolding. We proved that by modeling a tensile test, we could predict the bonding strength of the interface in overmolded parts with much higher accuracy than by averaging, which is widely used in similar calculations. The bonding strength of the interface modeled with our method differs from the measured results by less than 1%, while this difference is usually 10% or more in the case of averaging.

Our method combines the analytical modeling of reptation, the numerical modeling of overmolding, and the modeling of tensile tests. The unique features of the proposed method are:

- It takes into account the unevenness of temperature distribution on the contact surface during overmolding, and

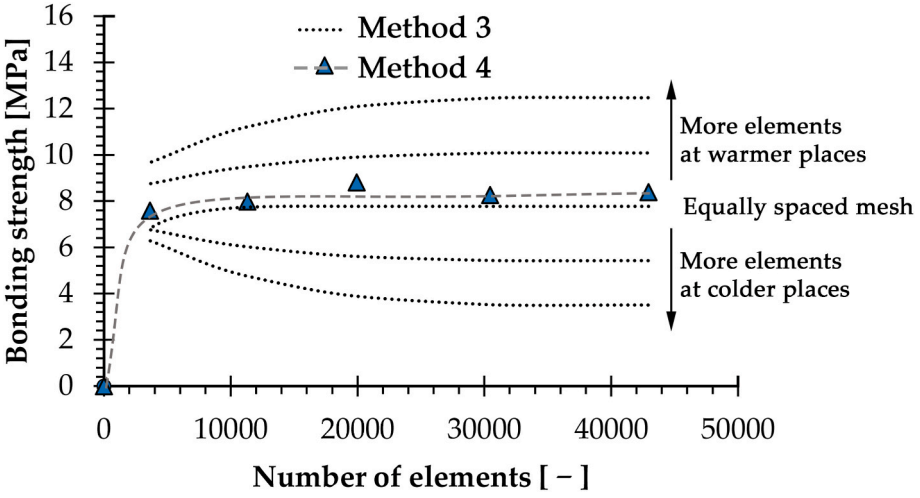

Fig. 25. Total bonding strength obtained by tensile test modeling in the case of an unequally spaced mesh.

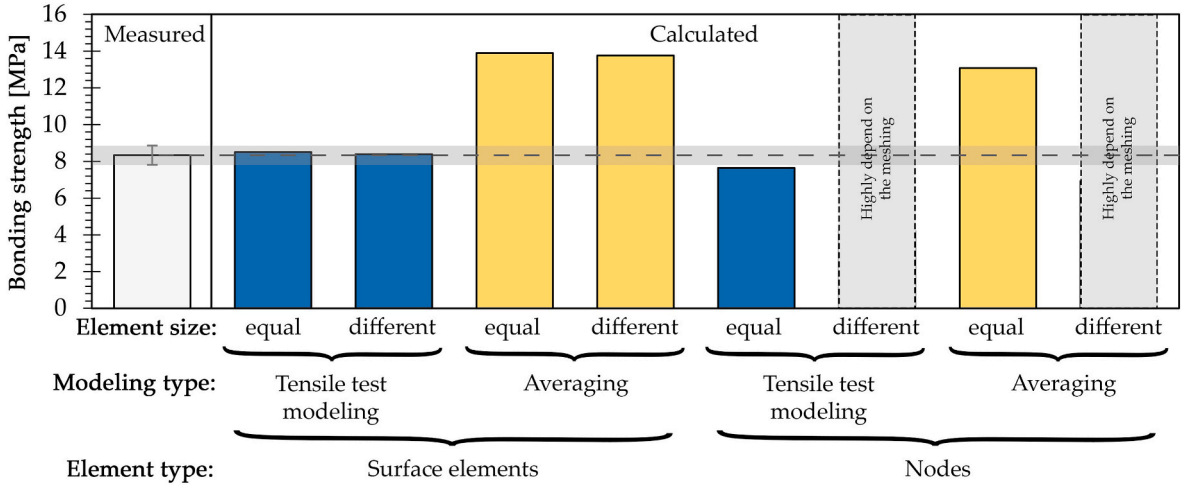

Fig. 26. Calculation method results for bonding strength with the measurement results (blue bar - results obtained by tensile test modeling, yellow bar - results obtained by averaging). (For interpretation of the references to colour in this figure legend, the reader is referred to the Web version of this article.)

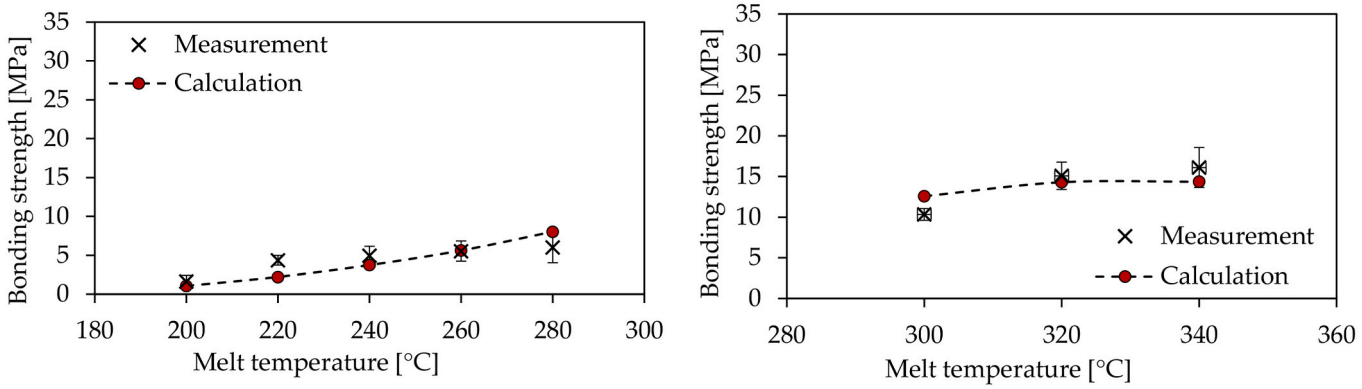

Fig. 27. Calculated and measured bonding strength of a) PS (Versalis Edistir N 3910) b) PC (Convestro Makrolon 2205).

- it models a tensile test, which describes the breaking process more realistically than the commonly used averaging method.

The proposed modeling method can be useful for engineers designing and producing overmolded parts.

Author contributions

Conceptualization, A.Sz. and J.G.K.; Methodology, A.Sz. and J.G.K.; Validation, J.G.K.; Investigation, A.Sz.; writing - original draft, A.Sz. and T.A.; Writing - review & editing, visualization, A.Sz., T.A. and J.G.K; project administration, J.G.K.; Funding acquisition and Supervision, J. G.K.

All authors have read and agreed to the published version of the manuscript.

Funding

Project no. C1548030 has been implemented with the support provided by the Ministry of Culture and Innovation of Hungary from the National Research, Development and Innovation Fund, financed under the KDP-2021 funding scheme. This work was supported by the National Research, Development and Innovation Office, Hungary (2020-1.2.3-EUREKA-2021-00010, 2019-1.1.1-PIACI-KFI-2019-00205, 2018-1.3.1-VKE-2018-00001). This research was funded by the Horizon Europe Framework Programme and the call HORIZON-WIDERA-2021-ACCESS-03, under the grant agreement for project 101079051 – IPPT_TWINN. The research was done under the scope of the Project no. RRF-2.3.1-21-2022-00009, entitled "National Laboratory for Renewable Energy" which has been implemented with the support provided by the Recovery and Resilience Facility of the European Union within the framework of Programme Széchenyi Plan Plus. Project no. TKP-6-6/PALY-2021 has been implemented with the support provided by the Ministry of Culture and Innovation of Hungary from the National Research, Development and Innovation Fund, financed under the TKP2021-NVA funding scheme."

Declaration of competing interest

The authors declare that they have no known competing financial interests or personal relationships that could have appeared to influence the work reported in this paper.

Data availability

The authors do not have permission to share data.

Acknowledgments

Moldex3D (CoreTech System Co., Ltd.) supported the research work professionally. We thank Arburg Hungária Kft. for the ARBURG Allrounder 470 A 1000–290 injection molding machine, Tool-Temp Hungária Kft., Lenzkes Gmbh, and Piovan Hungary Kft. for the accessories.

References

[1] A. Szuchács, T. Ageyeva, R. Boros, J.G. Kovács, Bonding strength calculation in multicomponent plastic processing technologies, Mater. Manuf. Process. 36 (2021) 1–9, https://doi.org/10.1080/10426914.2021.1948052.
[2] M.Z. Huang, J. Nomai, A.K. Schlarb, The effect of different processing, injection molding (im) and fused deposition modeling (fdm), on the environmental stress cracking (esc) behavior of filled and unfilled polycarbonate (pc), Expreess Polymer Letters 15 (2021) 194–202, https://doi.org/10.3144/expresspolymlett.2021.18.
[3] A. Stadlmann, A. Mautner, M. Pramreiter, A. Bismarck, U. Müller, Interfacial adhesion and mechanical properties of wood-polymer hybrid composites prepared by injection molding, Polymers 13 (2021) 2849, https://doi.org/10.3390/polym13172849.
[4] T. Schneider, Lightweight construction: first composite gearbox housing with layer-optimized organo sheeting weighs 30% less than a comparable aluminum component, Reinforc Plast 63 (2019) 40–45, https://doi.org/10.1016/j.repl.2017.11.018.
[5] G. Gardiner, Camisma's car seat back: hybrid composite for high volume. https://www.compositesworld.com/articles/camismas-car-seat-back-hybrid-composite-for-high-volume, 21 January 2020.
[6] R. Boros, P.K. Rajamani, J.G. Kovács, Combination of 3d printing and injection molding: overmolding and overprinting, Express Polym. Lett. 13 (2019) 889–897, https://doi.org/10.3144/expresspolymlett.2019.77.
[7] H.E. Quinlan, T. Hasan, J. Jaddou, A.J. Hart, Industrial and consumer uses of additive manufacturing: a discussion of capabilities, trajectories, and challenges, J. Ind. Ecol. 21 (2017) 15–20, https://doi.org/10.1111/jiec.12609.
[8] L. Pisanu, J. Barbosa, P. Bamberg, B. Marx, A. Schiebahn, R. Souza, M. Nascimento, Influence of coupling agents on the adhesion force of dissimilar overmolded polymers: a digital image correlation analysis, Materia 24 (2019), https://doi.org/10.1590/s1517-707620190003.0800.
[9] T. Geminger, S. Jarka, 4 - injection molding of multimaterial systems, in: H.-P. Heim (Ed.), Specialized Injection Molding Techniques, William Andrew Publishing, 2016, https://doi.org/10.1016/B978-0-323-34100-4.00004-3pp 165-210.
[10] M.-W. Wang, F. Arifin, V.-H. Vu, The study of optimal molding of a led lens with grey relational analysis and molding simulation, Period. Polytech. - Mech. Eng. 63 (2019) 278–294, https://doi.org/10.3311/PPme.13337.
[11] A. Benayad, R. El Otmani, A. El Hakimi, M. Boutaous, A. Touache, R.K. Musa, S. Derdouri, N. Mahfoudi, D. Siginer, Experimental investigation and numerical simulation of the microinjection molding process through an expanding flow configuration, Polym. Adv. Technol. 32 (2021) 1690–1711, https://doi.org/10.1002/pat.5206.
[12] A.C.A. Asseko, B. Cosson, E. Lafranche, F. Schmidt, Y. Le Maoult, Effect of the developed temperature field on the molecular interdiffusion at the interface in infrared welding of polycarbonate composite, Compos. B Eng. 97 (2016) 53–61, https://doi.org/10.1016/j.compositesb.2016.04.064.
[13] S. Ebnesajjad, Chapter 5 - theories of adhesion, in: S. Ebnesajjad (Ed.), Surface Treatment of Materials for Adhesive Bonding, second ed., William Andrew Publishing, Oxford, 2014, pp. 77–91, https://doi.org/10.1016/B978-0-323-26435-8.00005-8.
[14] P.G. de Gennes, Reptation of a polymer chain in the presence of fixed obstacles, J. Chem. Phys. 55 (1971) 572, https://doi.org/10.1063/1.1675789.

[15] L.J. Bastien, J.W. Gillespie, A non-isothermal healing model for strength and toughness of fusion bonded joints of amorphous thermoplastics, Polym. Eng. Sci. 31 (1991) 1720–1730, https://doi.org/10.1002/pen.760312406.
[16] F.O. Sonmez, H.T. Hahn, Analysis of the on-line consolidation process in thermoplastic composite tape placement, J. Thermoplast. Compos. Mater. 10 (1997) 543–572, https://doi.org/10.1177/089270579701000604.
[17] F. Yang, R. Pitchumani, Healing of thermoplastic polymers at an interface under nonisothermal conditions, Macromolecules 35 (2002) 3213–3224, https://doi.org/10.1021/ma010858o.
[18] R. Giusti, G. Lucchetta, Modeling the adhesion bonding mechanism in overmolding hybrid structural parts for lightweight applications, Key Eng. Mater. 611–612 (2014) 915–921. https://doi.org/10.4028/www.scientific.net/KEM.611-612.915.
[19] R. Giusti, G. Lucchetta, Modeling the adhesion bonding strength in injection overmolding of polypropylene parts, Polymers 12 (2020) 2063, https://doi.org/10.3390/polym12092063.
[20] R. Akkerman, M. Bouman, S. Wijskamp, Analysis of the thermoplastic composite overmolding process: interface strength, Frontier in Materials 7 (2020), https://doi.org/10.3389/fmats.2020.00027.
[21] E. Lafranche, S. Macedo, P. Ferreira, C.I. Martins, Thin wall injection-overmoulding of polyamide 6/polypropylene multilayer parts: Pa6/pp-g-ma interfacial adhesion investigations, Applied Polymer Science 138 (2020), https://doi.org/10.1002/app.50294.
[22] B. Jiang, L. Fu, M. Zhang, C. Weng, Z. Zhai, Effect of thermal gradient on interfacial behavior of hybrid fiber reinforced polypropylene composites fabricated by injection overmolding technique, Polym. Compos. 41 (2020) 4064–4073, https://doi.org/10.1002/pc.25693.
[23] B.-A. Behrens, K. Dröder, K. Brunotte, H. Wester, A. Hürkamp, T. Ossowski, R. Lorenz, Numerical modelling of bond strength in overmoulded thermoplastic composites, Journal of Composite Science 5 (2021) 164, https://doi.org/10.3390/jcs5070164, 164.
[24] B. Talamini, Y. Mao, L. Anand, Progressive damage and rupture in polymers, J. Mech. Phys. Solid. 111 (2018) 434–457, https://doi.org/10.1016/j.jmps.2017.11.013.
[25] L. Zhao, T. Qin, Y. Chen, J. Zhang, Three-dimensional progressive damage models for cohesively bonded composite π joint, J. Compos. Mater. 48 (2014) 707–721, https://doi.org/10.1177/0021998313477169.
[26] P.F. Liu, J.Y. Zheng, Recent developments on damage modeling and finite element analysis for composite laminates: a review, Mater. Des. 31 (2010) 3825–3834, https://doi.org/10.1016/j.matdes.2010.03.031.
[27] M. Teotia, R.K. Soni, Applications of finite element modelling in failure analysis of laminated glass composites: a review, Eng. Fail. Anal. 94 (2018), https://doi.org/10.1016/j.engfailanal.2018.08.016, 412-237.
[28] J.-H. Song, H. Wang, T. Belytschko, A comparative study on finite element methods for dynamic fracture, Comput. Mech. 42 (2007) 239–250, https://doi.org/10.1007/s00466-007-0210-x.
[29] G. Liu, T.E. Tay, V.B.C. Tan, Failure progression and mesh sensitivity analyses by the plate element-failure method, J. Compos. Mater. 44 (2010) 2363–2379, https://doi.org/10.1177/0021998310372466.